arXiv:0807.2643v2 [cond-mat.supr-con] 22 Jul 2008

Electronic Structure and Doping in $BaFe_2As_2$ and LiFeAs: Density Functional Calculations

D.J. Singh
Materials Science and Technology Division, Oak Ridge National Laboratory, Oak Ridge, Tennessee 37831-6114
(Dated: July 22, 2008)

We report density functional calculations of the electronic structure and Fermi surface of the $BaFe_2As_2$ and LiFeAs phases including doping via the virtual crystal approximation. The results show that contrary to a rigid band picture, the density of states at the Fermi energy is only weakly doping dependent and that the main effect of doping is a change in the relative sizes of the electron and hole Fermi surfaces as required by Luttinger's theory. This is a consequence of a change in As height with doping, in particular a shift of As towards Fe as holes are introduced in the Fe plane, as might be expected from simple ionic considerations. The main effect of doping is therefore a reduction in the degree of nesting of the Fermi surface. This provides a framework for understanding the approximate electron-hole symmetry in the phase diagrams of the Fe-As based superconductors.

PACS numbers:

I. INTRODUCTION

The discovery of high temperature superconductivity in oxypnictide phases, prototype LaFeAs(O,F) by Kamihara and co-workers[1] has sparked widespread interest in establishing the physical properties of these materials and especially the mechanism for superconductivity. This interest has led to the discovery of a number of new phases including other oxy-arsenides that when electron doped have critical temperatures exceeding 55K,[3] and hole doped superconducting phases including (K,Ba)Fe_2As_2, with T_c=38K[4,5] and Li_{1-y}FeAs with T_c of 18K.[6] Thus there are three families discovered so far: (1) the oxy-arsenides, spacegroup $P4/nmms$, with rare earth oxide layers separating the FeAs layers common to all of these superconductors, (2) the body centered tetragonal, $I4/mmm$ $ThCr_2Si_2$ structure materials ($BaFe_2As_2$), where the FeAs layers are stacked so that the As atoms face each other and the Ba atoms sit in the resulting 8-fold coordinated square prismatic sites between them, and (3) $P4/nmms$ LiFeAs, which is like the oxy-arsenide structure but with the rare earth oxide layers removed and replaced by Li (see below), resulting in a large decrease in the c-axis spacing of the FeAs layers. Stoichiometric (undoped) $BaFe_2As_2$ shows a spin density wave (SDW) type magnetic order and a structural transition with similar ordering temperatures. This feature is common to most of these materials, including the oxy-arsenides.[7,8] However, there are also some strong differences between properties of the oxypnictides and $BaFe_2As_2$. Most notable is the fact that with the exception of one report,[10] the oxy-arsenide superconductors are generally electron doped, while (Ba,K)Fe_2As_2 and Li_{1-y}FeAs are found to superconduct when hole doped. However, in both $BaFe_2As_2$ and LaFeAsO superconductivity apparently is associated with the suppression of the SDW. This is potentially of importance because there has been much discussion of the association between magnetic quantum critical points and high temperature superconductivity and in addition the specific spin fluctuations associated with the nesting that presumably drives the SDW have been studied as a possible pairing mechanism.[11]

Electronic structure studies,[12,13,14,15] show that the Fermi surfaces and band structures of these phases are qualitatively rather similar. In particular, all the compounds show small compensating electron and hole Fermi surfaces, but high densities of states. The hole Fermi surfaces occur around the zone center, and are generally derived from heavier (lower velocity) bands than the electron surfaces, which are around the zone corner (M point in a primitive tetragonal zone). Within band structure theories, moment formation is governed by a Stoner parameter, I, which takes values of 0.7 eV to 0.9 eV for ions near the middle of the 3d series (note that the effective I can reduced by hybridization). While magnetism may occur with lower values of the density of states, it must occur within a band picture if the Stoner criterion, $N(E_F)I > 1$, is met (the non-spin-polarized electronic structure becomes unstable against ferromagnetism in this case). Here $N(E_F)$ is the density of states (DOS) at the Fermi energy on a per atom per spin basis. The calculated values of $N(E_F)$ for the undoped FeAs materials put them at the borderline of itinerant magnetism, and in fact they are near both ferromagnetism, as required by the Stoner theory, and checkerboard antiferromagnetism, where nearest neighbor Fe atoms are oppositely polarized. The ground states, both experimentally[7,8,9] and theoretically[11,14,16,17,18,19] have a magnetic structure that corresponds to condensation of an M point (zone corner) SDW.

The electronic structures all show a strong increase in the electronic DOS as the Fermi energy is lowered into the heavier hole bands. This feature is quite robust in this family and is also the case for the corresponding phosphide compounds.[21,22] Importantly, this strong increase in the DOS poses a conundrum because it means that within a rigid band picture hole doped materials would be strongly magnetic, and therefore would necessarily have very different properties, including su-

perconductivity, from the electron doped materials. On the other hand, from an experimental point of view the generic phase diagram is much more symmetric, with an SDW and structural distortion near zero doping, with apparently non-magnetic, and superconducting states for both hole and electron doped materials. Here we investigate this issue using calculations for doped $BaFe_2As_2$ and LiFeAs within the virtual crystal approximation. This is an average potential approximation, which is beyond the rigid band method. We in fact find strong non-rigid band effects that leave only a weak doping level dependence to the $N(E_F)$ and provide a plausible explanation for the generic phase diagram of this family of materials.

II. STRUCTURE AND METHOD

The present calculations were performed within the local density approximation (LDA) using the general potential linearized augmented planewave (LAPW) method,[26] similar to those reported previously for LaFeAsO.[12] LAPW sphere radii of 1.8 a_0, 2.2 a_0, 2.1 a_0, and 2.1 a_0 were used for Li, Ba, Fe and As, respectively. The effect of doping was included by the virtual crystal approximation, by varying the nuclear charge of Ba or Li. Importantly, the internal parameters, including the As and Li positions, were relaxed independently for each doping level.

We took the experimental tetragonal lattice parameters of room temperature $BaFe_2As_2$ of Ref. 4, and relaxed the internal coordinate of As using LDA total energy minimization. The calculated coordinate is z_{As}=0.342. This is noticeably lower than the reported value of z_{As}=0.3545. In fact the As heights in these two structures differ by 0.16 Å, which as discussed below is outside the normal range of density functional errors and is significant for the electronic structures. We also did calculations with the generalized gradient approximation but find a similar discrepancy. Similar discrepancies have also been noted in the LaFeAsO series.[19,23] For LiFeAs, we used the experimental lattice parameters[24] and relaxed the free internal coordinates. The experimental structure (spacegroup $P4/nmms$, 129) shows two Li sites: 2c, which according to Ref. 24 is fully occupied, and lies above and below the centers of the Fe squares opposite the As, as shown in Fig. 1, and 2b which has a reported occupancy of 0.1 in $Li_{1.1}FeAs$ and lies directly above the Fe. We performed total energy calculations for stoichiometric LiFeAs with Li in the 2b and 2c sites and found that the 2c site is favored by 0.52 eV per formula unit. Accordingly, we performed our doping studies placing Li in the 2c site. We note that while this is the opposite choice to that made by Nekrasov and co-workers[15], the electronic structure near the Fermi energy is practically unaffected by this choice. In fact, when hole doped by Li vacancies one may expect Coulomb repulsions between the like charged Li ions to favor partial occupations of the 2b site, though always with a higher occupancy on the 2c site, similar to what is found in Na_xCoO_2. In any case, the insensitivity of the electronic structure to the Li position supports the validity of the virtual crystal approximation. The structures that we used for the undoped compounds are summarized in Table I.

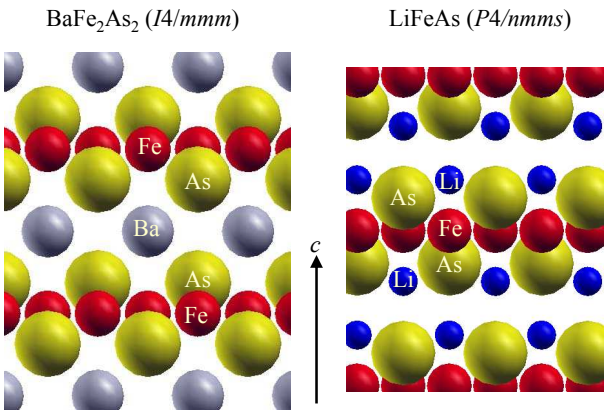

FIG. 1: (Color online) Crystal structure of $BaFe_2As_2$ (left) and LiFeAs (right) with the relaxed As and Li coordinates. Note that in both structures the FeAs layers are uniformly spaced along the c-axis direction.

TABLE I: Structures used in calculations for undoped $BaFe_2As_2$ and LiFeAs.

	$BaFe_2As_2$	LiFeAs
Spacegroup	$I4/mmm$	$P4/nmms$
a(Å)	3.9625	3.776
c(Å)	13.0168	6.349
z_{As}	0.3545	0.2116
z_{Li}		0.6728
d(As-Fe)(Å)	2.315	2.403

III. UNDOPED REFERENCE SYSTEMS

The calculated LDA band structures and electronic DOS for $BaFe_2As_2$ are given in Figs. 2 and 3, respectively. These were calculated using the LDA relaxed As height as given in Table I. The Fermi surfaces for the calculated As height are depicted in Figs. 6 and 7. As noted previously,[13,15] They consist of electron cylinders at the zone center and hole cylinders and other sections that depend strongly on the As height at the zone center. For $BaFe_2As_2$ the hole Fermi surface flares out at k_z=1/2 (Z), giving it a more three dimensional character than that of the Li compound. This flaring out is sensitive to the As height, and in particular is reduced as the As is moved away from the Fe plane. In the Li compound there are three hole sections. These are two very two dimensional hole cylinders and an inner surface that forms a capped cylinder centered at Γ. Calculations were also done for the experimental As height (Fig. 3).

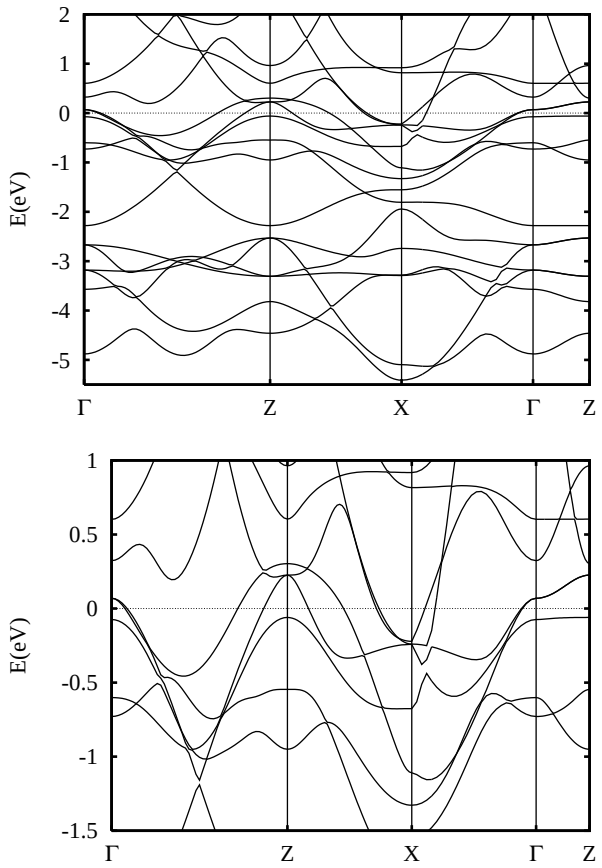

FIG. 2: Calculated LDA band structure of $BaFe_2As_2$ for the LDA value of z_{As}. The lower panel shows a blow-up near E_F, which is set to 0 eV. The short Γ-Z direction is from [0,0,0] to [0,0,1/2] while the long Γ-Z is in the basal plane and runs from [0,0,0] to [1,0,1/2] in units of the body centered tetragonal primitive reciprocal lattice vectors.

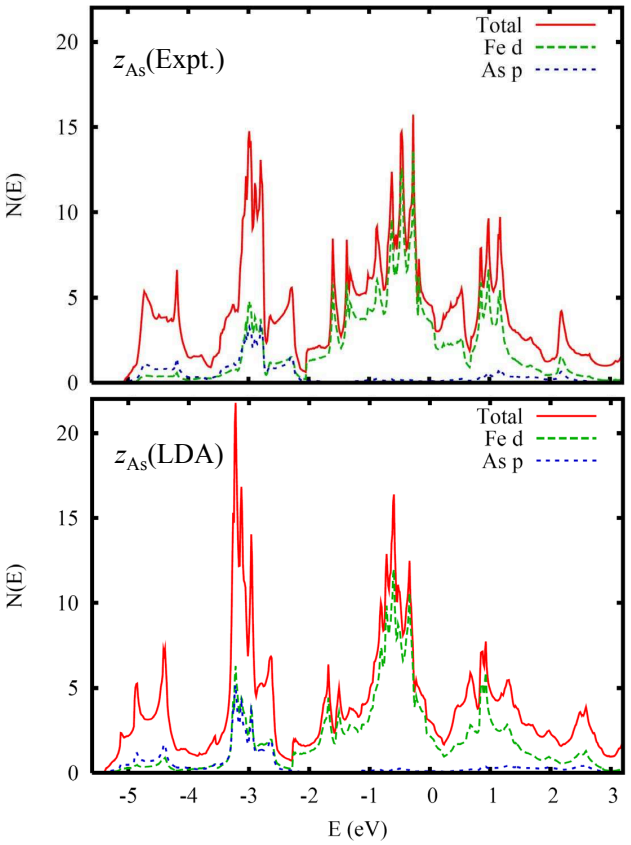

FIG. 3: (color online) Calculated electron DOS of $BaFe_2As_2$ for the experimental (top) and LDA (bottom) values of z_{As}, plotted on a per formula unit basis. The projections are onto the LAPW spheres. Since As has extended p orbitals that extend well beyond the LAPW sphere, this yields values that are proportional to the As contribution, but underestimate it.

These lead to a significantly higher $N(E_F)$, which will make the material more magnetic, as has been discussed for the oxy-arsenide materials.[19,23] The band structure and DOS for LiFeAs are given in Figs. 4 and 5, respectively, again using the calculated internal coordinates. The calculated values of $N(E_F)$ are 3.06 eV^{-1} per formula unit (two Fe atoms) both spins for $BaFe_2As_2$ and 3.58 eV^{-1} for LiFeAs on a per unit cell (two Fe atoms, two formula units), both spins basis. For the experimental z_{As}=0.3545 of $BaFe_2As_2$ we obtain $N(E_F)$ = 4.59 eV^{-1} per formula unit. These values are lower than the corresponding value for LaFeAsO (2.62 eV^{-1} per Fe both spins).[12] but are still high enough to place the materials near magnetism.

For $BaFe_2As_2$ we find an antiferromagnetic state corresponding to the SDW to be the most stable of the states considered. For the LDA value of z_{As} we do not find any instability against either a ferromagnetic or a checkerboard (nearest neighbor) antiferromagnetic state in the LDA. The SDW state, which consists of lines of parallel spin Fe atoms in the FeAs planes has a moment defined by the integral inside the Fe LAPW sphere, radius 2.1 a_0, of 0.7 μ_B. As mentioned, $N(E_F)$ is larger when the As height is raised to the reported experimental value leading to a more magnetic state. In this case, within the LDA we find a very weak instability of the non-spin-polarized state to ferromagnetism (0.3 μ_B/Fe, 0.01 meV/Fe). a stronger instability for the checkerboard antiferromagnetism (1.6 μ_B/Fe, 41 meV/Fe) and the strongest instability to the SDW, which is the ground state (1.75 μ_B/Fe, 92 meV/Fe). For the experimental value of z_{As} the state with ferromagnetic c-axis stacking of the Fe in the SDW state has higher energy, and is therefore less stable than the state with antiferromagnetic stacking, by 3 meV/Fe, while these two states are degenerate to the precision of the calculation for the LDA As height. Thus the lowest energy magnetic structure that we find is the SDW ordering in the Fe layers, stacked so that Fe atoms directly above each other in the c-direction are antiferromagnetically aligned. This is in accord with recent experimental results.[28] The high sensitivity of the Fe moment to the ordering and the fact that the SDW state is so much lower in energy than any other

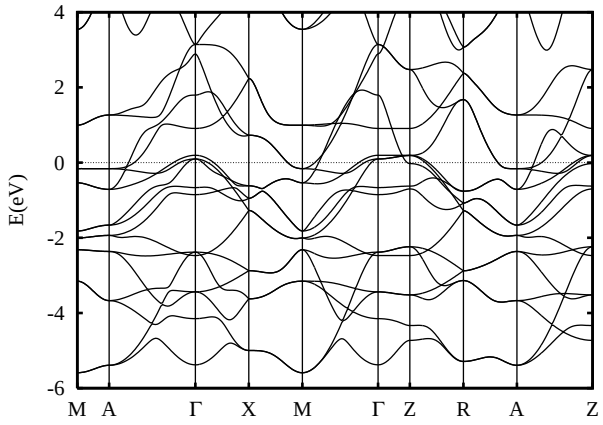

FIG. 4: Calculated LDA band structure of LiFeAs for the LDA internal coordinates.

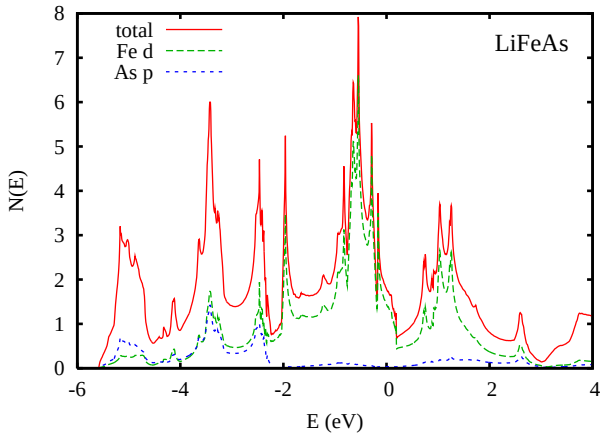

FIG. 5: (color online) Calculated electron DOS of LiFeAs for the LDA internal coordinates, on a per formula unit basis. Note that the formula unit for this compound contains one Fe, while that for $BaFe_2As_2$ contains two.

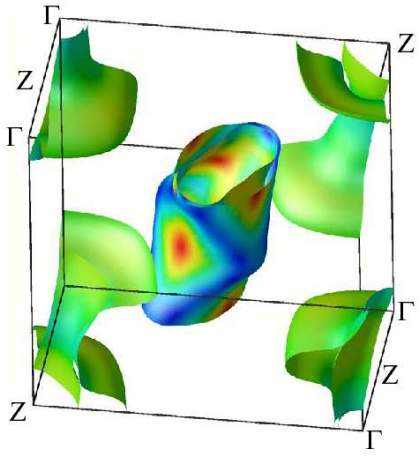

FIG. 6: (color online) LDA Fermi surface of $BaFe_2As_2$ for the LDA internal coordinates, shaded by band velocity.

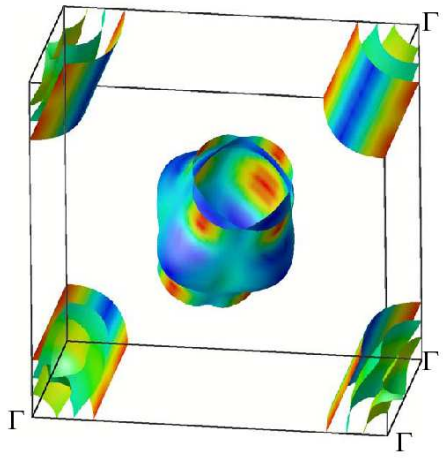

FIG. 7: (color online) LDA Fermi surface of LiFeAs for the LDA internal coordinates, shaded by band velocity.

magnetic state strongly imply that the magnetism is of itinerant character with a spin density wave driven by the structure of the Fermi surface rather than local moment physics associated with Heisenberg type exchange couplings.

These undoped electronic structures are similar to those obtained previously and show the generic features of the calculated electronic structures of the other FeAs materials – small Fermi surfaces, with hole cylinders at the zone center and electron cylinders at the zone corner, high $N(E_F)$, and a strongly increasing DOS below E_F. The somewhat lower values of $N(E_F)$ compared to LaFeAsO would place $BaFe_2As_2$ and LiFeAs further from ferromagnetism. This combined with the fact that ferromagnetic spin fluctuations are highly pair breaking for singlet superconducting states may partially explain why hole doping is effective in these non-oxide materials, but the large increase in the DOS below E_F works against this explanation taken by itself.

IV. DOPED MATERIALS: VIRTUAL CRYSTAL CALCULATIONS

In this section we report virtual crystal calculations for the two compounds. This approach differs from rigid band in that it includes the self-consistent rearrangement of the charge density, which is done in an average potential. This approximation is justified since the Ba and Li states do not contribute in any significant way to the band structure near E_F and because the scattering due to disorder on the Ba and Li sites is expected to be weak in view of the fact that wavefunctions of the states near E_F are primarily Fe derived and therefore separated from the Ba/Li atoms. This is supported by the fact that, as mentioned, we find no noticeable difference in the electronic structure as calculated with the Li atoms of LiFeAs in sites $2b$ and $2c$. Importantly, in the present context, we

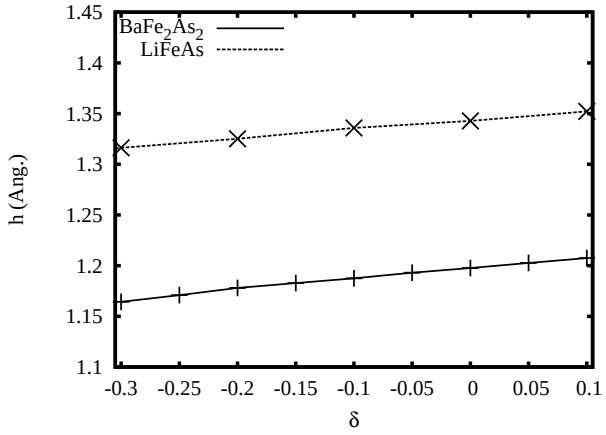

FIG. 8: Calculated As height as a function of virtual crystal doping, δ in carriers per Fe. Negative δ corresponds to hole doping.

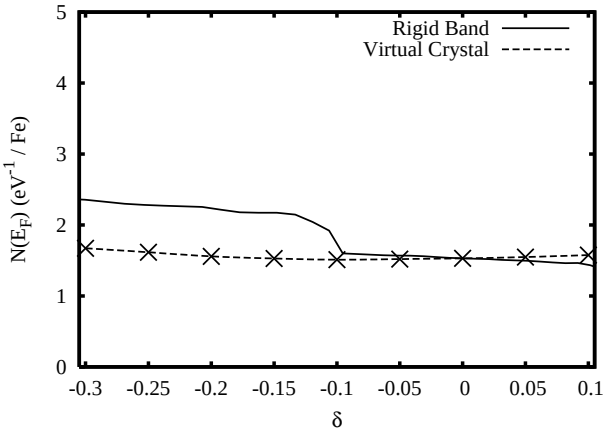

FIG. 9: Rigid band DOS as compared to the virtual crystal $N(E_F)$ as a function of doping level for $BaFe_2As_2$. Note that the doping levels given in carriers per Fe with negative indicating hole doping, and the $N(E_F)$ are given on a per Fe atom basis.

are able to relax the internal coordinates and in particular the As heights in the virtual crystal approximation.

The calculated As height above the Fe plane as a function of doping is shown in Fig. 8. As may be seen, the As drops towards the Fe plane as holes are introduced. This is as might be anticipated for a primarily ionic situation, since a more highly positively charged Fe layer will be more attractive to As^{3-} and since the effective size of transition element ions in solids decreases as the valence increases.[29,30] The essential point is that in these materials the carrier density is relatively low with an electronic structure near E_F formed from band edges. As a result the DOS and Fermi surface are sensitive to small changes, including the As position.

Figs. 9 and 10 show the calculated virtual crystal values of $N(E_F)$ for various doping levels as a function of doping level. As may be seen the behavior of the virtual

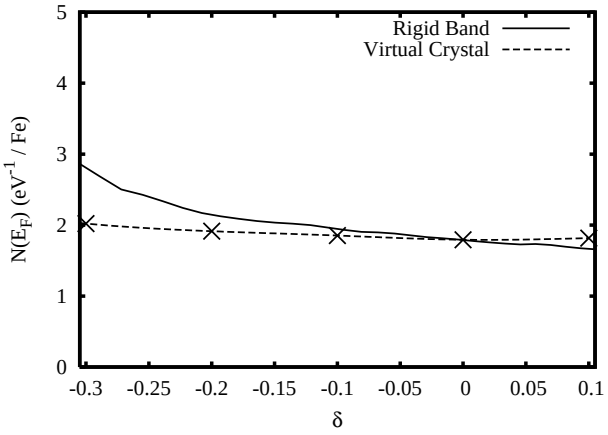

FIG. 10: Rigid band DOS as compared to the virtual crystal $N(E_F)$ as a function of doping level for LiFeAs. Note that the doping levels given in carriers per Fe with negative indicating hole doping, and the $N(E_F)$ are given on a per Fe atom basis.

crystal is very different from what may be expected from a rigid band viewpoint. In particular, $N(E_F)$ is found to be very nearly constant over the doping range studied, while as mentioned, the rigid band point of view would lead one to expect an increasing $N(E_F)$ upon hole doping. Our result differs from that of a recent calculation of Shein and Ivanovskii,[31] who studied a supercell of composition $Ba_{0.5}K_{0.5}Fe_2As_2$, and found a significant increase in $N(E_F)$ relative to the undoped compound. We ascribe this difference to the fact that they used the fixed experimental As position for the undoped compound and did not relax the internal coordinates. In any case, we find that contrary to the rigid band picture hole doping does not bring the system closer to Stoner ferromagnetism, which as mentioned would be detrimental to superconductivity. Thus the main effects on the electronic structure are more subtle.

Figs. 11 and 12 show the evolution of the non-spin-polarized virtual crystal Fermi surface for the two compounds. As may be seen the basic structure of the Fermi surface with hole sections around the zone center and electron sections at the zone corner is maintained for all the doping levels shown. The difference between the volume of the hole and electron sections is required to correspond to the doping level by the Luttinger theorem. Also it may be seen that the size of the electron sections changes at least as much as that of the hole sections (note that in Fig. 11 the top view emphasizes the flaring out of the hole Fermi surface at k_z=0.5, while the main cylindrical sections are smaller). This is contrary to what might be anticipated considering that the electron bands are more dispersive than the hole bands and therefore should change less and again shows the importance of non-rigid band effects.

The condition for an SDW instability of the paramagnetic state is that the real part of the susceptibility, $\chi(\mathbf{q})$ should diverge at the nesting vector. This function

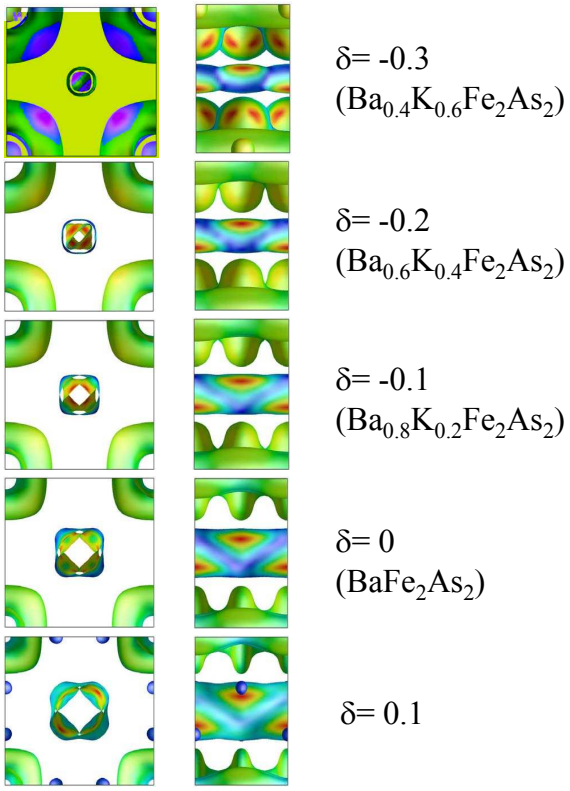

FIG. 11: (color online) Virtual crystal Fermi surface of $BaFe_2As_2$ as a function of doping level δ using the relaxed As position for each value of δ. The shading is by velocity. The left panels show a view along the k_z directions, while the right panels are along k_x.

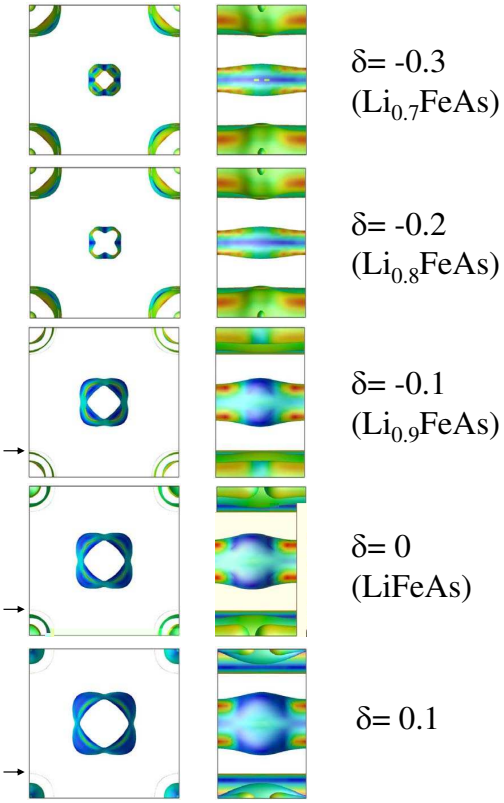

FIG. 12: (color online) Virtual crystal Fermi surface of LiFeAs as a function of doping level δ using the relaxed atomic positions for each value of δ. The shading is by velocity. The left panels show a view along the k_z directions, while the right panels are along k_x. The outermost hole cylinder is very two dimensional and therefore is difficult to see in the view along k_z. Accordingly we indicate its position by an arrow.

is given in terms of an integral over the Fermi surface for the bare Lindhard susceptibility, $\chi_0(\mathbf{q})$, with an enhancement factor that emphasizes peaks, much like the Stoner enhancement of the Pauli susceptibility for the ferromagnetic case. The interband Lindhard susceptibility for an electron cylinder at the zone corner and a same sized hole cylinder at the zone center is a function peaked at the nesting vector, while if the cylinders differ in radius by δq, e.g. due to doping or extra hole sections, the function will have a flat cylindrical plateau centered at the former nesting vector with diameter $2\delta q$. Thus as the cylinders become mismatched in size the maximum value of $\chi_0(\mathbf{q})$ (the value at the nesting vector) will decrease, while a region of high constant $\chi_0(\mathbf{q})$ will develop within δq of the nesting vector.

We calculated the Lindhard function, setting all matrix elements to be equal (i.e. constant matrix element approximation yielding arbitrary units). Although the Fermi surfaces are not perfect cylinders and there are multiple surfaces of different size, we do in fact find this behavior for LiFeAs. It is also the case for electron doping in $BaFe_2As_2$ and to a lesser degree for hole doped $BaFe_2As_2$, where the peak in $\chi_0(\mathbf{q})$ becomes broader and smaller but there is no clear plateau region. For both LiFeAs and $BaFe_2As_2$ we find a decrease in the peak height of the Lindhard function as we dope with holes. This explains why the SDW is destroyed by hole doping in these materials.

V. DISCUSSION

There has been much recent discussion of the relationship between the SDW instability and superconductivity. Within an Eliashberg formalism involving spin fluctuations what enters the calculation of the pairing function is a double integral over the Fermi surface (like that in the Lindhard function) with a kernel containing the pairing interaction, $V(\mathbf{q}) \sim \chi(\mathbf{q})$. Thus in the case discussed above, the interband superconducting pairing between the electron and hole Fermi surfaces will depend on an integral over a range of $\mathbf{q}$ of size comparable to the Fermi surface size, while the SDW instability will depend on the peak value of $\chi(\mathbf{q})$ (in a real case spin fluctuations

away from the SDW ordering vector will compete with the SDW so even for a given maximum value of the bare $\chi_0(\mathbf{q})$ a system with a narrower peak will order first). In any case, if spin fluctuations associated with the SDW are responsible for pairing, one expects superconductivity to compete with the SDW and to occur on both sides of the region where the SDW is stable. What our results show is that the properties are much more symmetric between hole and electron doping than would be expected from a rigid band picture.

Acknowledgments

We are grateful for helpful discussions with I.I. Mazin, M.H. Du, D.G. Mandrus and B.C. Sales. This work was supported by the Department of Energy, Division of Materials Sciences and Engineering.

[1] Y. Kamihara, T. Watanabe, M. Hirano, and H. Hosono, J. Am. Chem. Soc. **130**, 3296 (2008).
[2] Z.A. Ren, W. Lu, J. Yang, W. Yi, X.L. Shen, Z.C. Li, G.C. Che, X.L. Dong, L.L. Sun, F. Zhou, and Z.X. Zhao, Chin. Phys. Lett. **25**, 2215 (2008).
[3] C. Wang, L. Li, S. Chi, Z. Zhu, Z. Ren, Y. Li, Y. Wang, X. Lin, Y. Luo, S. Jiang, X. Xu, G. Cao, and Z. Xu, arXiv:0804.4290 (2008).
[4] M. Rotter, M. Tegel, D. Johrendt, I. Schellenberg, W. Hermes, and R. Pottgen, arXiv:0805.4021 (2008).
[5] M. Rotter, M. Tegel, and D. Johrendt, arXiv:0805.4630 (2008).
[6] X.C. Wang, Q.Q. Liu, Y.X. Lu, W.B. Gao, L.X. Yang, R.C. Yu, F.Y. Li, and C.Q. Jin, arXiv:0806.1687 (2008).
[7] C. de la Cruz, Q. Huang, J.W. Lynn, J. Li, W. Ratcliff II, J.L. Zaretsky, H.A. Mook, G.F. Chen, J.L. Luo, N.L. Wang, and P. Dai, arXiv:0804.0795 (2008).
[8] Q. Huang, Y. Qiu, W. Bao, J.W. Lynn, M.A. Green, Y.C. Gasparovic, T. Wu, G. Wu, and X.H. Chen, arXiv:0806.2776 (2008).
[9] A.I. Goldman, D.N. Argyriou, B. Ouladdiaf, T. Chatterji, A. Kreyssig, S. Nandi, N. Ni, S.L. Budko, P.C. Canfield, and R.J. McQueeney, arXiv:0807.1525 (2008).
[10] H.-H. Wen, G. Mu, L. Fang, H. Yang, and X. Zhu, Europhys. Lett. **82**, 17009 (2008).
[11] I.I. Mazin, D.J. Singh, M.D. Johannes, and M.H. Du, arXiv:0803.2740 (2008).
[12] D.J. Singh and M.H. Du, Phys. Rev. Lett. **100**, 237003 (2008).
[13] I.A. Nekrasov, Z.V. Pchelkina, and M.V. Sadovskii, arXiv:0806.2630 (2008).
[14] F. Ma, Z.Y. Lu, and T. Xiang, arXiv:0806.3526 (2008).
[15] I.A. Nekrasov, Z.V. Pchelkina, and M.V. Sadovskii, arXiv:0807.1010 (2008).
[16] J. Dong, H.J. Zhang, G. Xu, Z. Li, G. Li, W.Z. Hu, D. Wu, G.F. Chen, X. Dai, J.L. Luo, Z. Fang, and N.L. Wang, Europhys. Lett. **83**, 27006 (2008).
[17] F. Ma and Z.Y. Lu, arXiv:0803.3286 (2008).
[18] T. Yildirim, arXiv:0804.2252 (2008).
[19] Z.P. Yin, S. Lebegue, M.J. Han, S.Y. Savrasov, and W.E. Pickett, arXiv:0804.3355 (2008).
[20] L.X. Yang, H.W. Ou, J.F. Zhao, Y. Zhang, D.W. Shen, B. Zhou, J. Wei, F. Chen, M. Xu, C. He, X.F. Wang, T. Wu, G. Wu, Y. Chen, X.H. Chen, Z.D. Wang, and D.L. Feng, arXiv:0806.2627 (2008).
[21] S. Lebegue, Phys. Rev. B **75**, 035110 (2007).
[22] E. Gustenau, P. Herzig, and A. Neckel, J. Alloys Compds. **262-263**, 516 (1997).
[23] I.I. Mazin, M.D. Johannes, L. Boeri, K. Koepernik, and D.J. Singh, Phys. Rev. B (in press).
[24] R. Juza and K. Langer, Z. Anorg. Allg. Chem. **361**, 58 (1968).
[25] Z.W. Zhu, Z.A. Xu, X. Lin, G.H. Cao, C.M. Feng, G.F. Chen, Z. Li, J.L. Luo, and N.L. Wang, arXiv:0804.1324
[26] D.J. Singh and L. Nordstrom, *Planewaves, Pseudopotentials and the LAPW Method, 2nd. Ed.* (Springer, Berlin, 2006).
[27] D. Singh, Phys. Rev. B **43**, 6388 (1991).
[28] Y. Su, P. Link, A. Schneidewind, T. Wolf, Y. Xiao, R. Mittal, M. Rotter, D. Johrendt, T. Brueckel, and M. Loewenhaupt, arXiv:0807.1743 (2008).
[29] L. Pauling, *The Nature of the Chemical Bond and the Structure of Molecules and Crystals: An Introduction to Modern Structural Chemistry, 3rd ed.* (Cornell University Press, Ithaca, 1960).
[30] R.D. Shannon, Acta Cryst. **A32**, 751 (1972).
[31] I.R. Shein and A.L. Ivanovskii, arXiv:0807.0984 (2008).